

Contextual Modeling of Functional MR Images With Conditional Random Fields

Yang Wang, *Member, IEEE*, and Jagath C. Rajapakse* , *Senior Member, IEEE*

Abstract—This paper presents a conditional random field (CRF) approach to fuse contextual dependencies in functional magnetic resonance imaging (fMRI) data for the detection of brain activation. The interactions among both activation (activated/inactive) labels and observed data of brain voxels are unified in a probabilistic framework based on the CRF, where the interaction strength can be adaptively adjusted in terms of the data similarity of neighboring sites. Compared to earlier detection methods, including statistical parametric mapping and Markov random field, the proposed method avoids the suppression of high frequency information and relaxes the strong assumption of conditional independence of observed data. Experimental results show that the proposed approach effectively integrates contextual constraints within the detection process and robustly detects brain activities from fMRI data.

Index Terms—Brain activation, conditional random field (CRF), functional magnetic resonance imaging (fMRI), Markov random field (MRF), statistical parametric mapping (SPM).

I. INTRODUCTION

FUNCTIONAL magnetic resonance imaging (fMRI) is a popular technique that noninvasively studies brain functions under various cognitive and behavioral tasks. Functional brain studies acquire a time-series of brain scans while the subject is alternatively performing an experimental task and a baseline task (so that the input stimulus to the brain takes the form of an on-off box-car pattern). Brain regions of interest are then detected through measuring the oxygenation level variations in blood vessels near the neurons activated by the input stimulus, i.e., the blood-oxygenation-level-dependent (BOLD) contrast. In fMRI experiments, the BOLD signal changes resulted from neural activities are usually close to the noise level. Hence, it is important to develop analysis methods that can robustly detect activated brain regions from the noisy fMRI time-series. Both model-based approaches and model-independent (or data-driven) approaches that classify or segment brain voxels into active and inactive areas have been extensively studied for the analysis of fMRI data.

In model-based methods, a statistical parametric map of brain activation is built by examining the time-series response of each voxel in the brain, given the information about the stimula-

tion. The significance of activation can be assessed using various statistical models including correlation analysis [2], [10], t-test or F-test [12], permutation [22], and mixture model [8], [28]. Recently, probabilistic graphical models such as Bayesian network and hidden semi-Markov event sequence model have also been employed to characterize fMRI time-series [9], [20]. On the other hand, data-driven methods such as clustering analysis [13], principal component analysis [14], and independent component analysis [5] attempt to reveal components of interest from the fMRI data without requiring the knowledge of the activation temporal response. However, the physiological meaning of the results is usually hard to explain, and it is difficult to perform statistical significance analysis based on data-driven methods. This paper deals with fMRI analysis from a probabilistic point of view by using a model-based method.

Besides local information measured at individual brain voxels, the strategy to effectively fuse contextual dependencies within functional imaging data is a key factor for the detection of brain activation [15]. For instance, it is known that the regions of interest usually consist of a number of contiguous brain voxels [6]. Since neighboring sites are likely to belong to the same class, spatial smoothing or filtering can be used in the preprocessing of fMRI data to enhance the overall signal-to-noise ratio (SNR) in activated regions. However, linear filtering suppresses high frequency information in fMRI data and may cause small activated regions undetectable. The notion of Markov random field (MRF), which is originally proposed for direct modeling of spatial interaction in image data [3], has been introduced to encourage contiguous results of activity detection by defining pairwise potentials between neighboring activation (activated/inactive) labels [7], [24], [25]. In these MRF approaches, spatial regularization and activity detection are simultaneously handled to enhance the performance of fMRI data analysis. MRF has also been employed to impose smoothness constraint on brain regions with different characteristics of hemodynamic response function (HRF) [26]. However, conditional independence of observations is usually assumed in MRF approaches so that interactions among observed data are ignored when activation labels are given. Because of the interconnection within brain areas, the time-series of an activated brain voxel is highly dependent on its activated neighbors. Therefore, the strong assumption of conditional independence is too restrictive for the modeling of functional images in fMRI analysis.

Compared to generative models including MRF and hidden Markov model, the conditional random field (CRF) models the contextual dependencies in a probabilistic discriminative framework that directly considers the posterior distribution over labels given observations [18], which relaxes the strong inde-

Manuscript received March 3, 2006; revised March 22, 2006. Asterisk indicates corresponding author.

Y. Wang is with the BioInformatics Research Centre, School of Computer Engineering, Nanyang Technological University, Singapore 639798 (e-mail: yang.wang@ieee.org).

J. C. Rajapakse is with the BioInformatics Research Centre, School of Computer Engineering, Nanyang Technological University, Singapore 639798, and also with Biological Engineering Division, Massachusetts Institute of Technology, Cambridge, MA 02139 USA (e-mail: asjagath@ntu.edu.sg).

Digital Object Identifier 10.1109/TMI.2006.875426

pendence assumption and captures neighborhood interactions among observations. Originally proposed for one-dimensional text sequence labeling, CRF has been applied to image and video labeling recently [17], [27].

Based on the CRF, this paper presents a probabilistic approach for the detection of brain activity from fMRI data. The contextual dependencies of both activation labels and observed data of brain voxels are unified in a probabilistic discriminative framework, where the interaction strength is adaptively adjusted according to the similarity between neighboring sites. The dependencies of data in functional MRI may come from spatial coupling of hemodynamic responses or correlated noises. Given the observed data, the posterior distribution over the activation labels is maximized by mean field approximation. Experimental results show that the proposed approach effectively integrates contextual constraints in functional images and significantly improves the robustness of the activity detection in fMRI data.

The rest of the paper is arranged as follows: Section II presents the CRF approach and compares it with the MRF method for the contextual modeling of functional imaging data. Section III proposes the activity detection algorithm for fMRI analysis. Section IV describes the implementation details. Section V discusses the experimental results. Then our technique is concluded in Section VI.

II. MODEL REPRESENTATION

For a pixel (or voxel) x within a two-dimensional (2-D) [or three-dimensional (3-D)] image, the activation label and observed data of the point are denoted by l_x and d_x respectively. Label $l_x \in \{0, 1, \dots, L-1\}$ assigns each point x to one of L regions (or classes) composing the scene. Here $L \in \mathbf{N}$ ($L = 2$ in this paper), $x \in X$, and X is the spatial domain of the scene. The observation d_x consists of measured information at the site x . The entire activation pattern (or label field) and observed data over the scene are compactly expressed as \mathbf{l} and \mathbf{d} , respectively.

Given the observed data, there are two ways to estimate the activation labels. The probabilistic generative framework considers the joint distribution over labels and observations. Using the Bayes' rule, the posterior probability of the activation pattern is expressed as $p(\mathbf{l}|\mathbf{d}) \propto p(\mathbf{l}, \mathbf{d}) = p(\mathbf{l})p(\mathbf{d}|\mathbf{l})$. Hence, the prior $p(\mathbf{l})$ and the likelihood $p(\mathbf{d}|\mathbf{l})$ should be formulated individually to estimate the posterior $p(\mathbf{l}|\mathbf{d})$. Alternatively, the probabilistic discriminative framework directly considers the posterior distribution of the activation pattern $p(\mathbf{l}|\mathbf{d})$. In this paper, the contextual constraints for the activity detection are imposed through a discriminative framework of statistical dependencies among neighboring sites.

A. CRF Formulation

To incorporate interactions among both labels and observations into the detection of brain activation, the posterior probability $p(\mathbf{l}|\mathbf{d})$ is formulated by a CRF. CRF is originally proposed in the discriminative framework avoiding the formulation of observation model. The definition of CRF is given by Lafferty *et al.* [18]. For observed data \mathbf{d} and corresponding labels \mathbf{l} over the scene, (\mathbf{l}, \mathbf{d}) is a CRF if, when conditioned on \mathbf{d} , the random field \mathbf{l} obeys the Markov property: $p(l_x|\mathbf{d}, l_y, y \neq x) = p(l_x|\mathbf{d}, l_y, y \in N_x)$, where set N_x denotes the neighboring sites

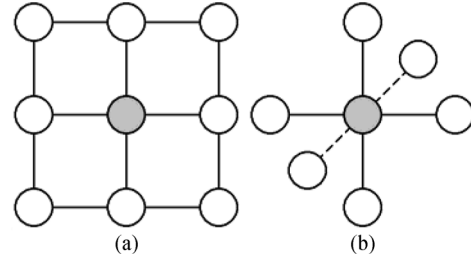


Fig. 1. (a) The 8-pixel neighborhood. (b) The 6-voxel neighborhood.

of point x (e.g., see Fig. 1). Using the Hammersley-Clifford theorem and considering up to pairwise clique potentials, the posterior distribution can be expressed as a Gibbs distribution with the following form [4]:

$$p(\mathbf{l}|\mathbf{d}) \propto \exp \left\{ - \sum_{x \in X} \left[V_x(l_x|\mathbf{d}) + \sum_{y \in N_x} V_{x,y}(l_x, l_y|\mathbf{d}) \right] \right\}. \quad (1)$$

The one-pixel potential $V_x(l_x|\mathbf{d})$ imposes the local constraint for a single site. Meanwhile the two-pixel potential $V_{x,y}(l_x, l_y|\mathbf{d})$ models the contextual information (or pairwise constraint) between neighboring sites. Strength of the constraints is dependent on the observed data. The potential functions are further expressed as

$$V_x(l_x|\mathbf{d}) = V_x^l(l_x) + V_x^{ld}(l_x|\mathbf{d}), \quad (2a)$$

$$V_{x,y}(l_x, l_y|\mathbf{d}) = V_{x,y}^l(l_x, l_y) + V_{x,y}^{ld}(l_x, l_y|\mathbf{d}). \quad (2b)$$

In the one-pixel potential, the first term reflects the prior knowledge for different label classes, and the second term reflects the observed information from individual sites. In the two-pixel potential, the first term imposes the connectivity constraint independent of the observations, and the second term imposes the neighborhood interaction dependent on the observed data. Thus, during the detection process both the data-independent and data-dependent contextual dependencies are unified in a probabilistic discriminative framework based on the CRF. The CRF approach will degenerate into a MRF approach when the data-dependent pairwise potential is set to zero (see the next part in this section), which is equivalent to the conditional independence assumption of the observed data (i.e., ignore interactions among observations when labels are given) used in previous approaches [24], [25].

B. Motivation

In a generative framework, the prior probability of the activation pattern $p(\mathbf{l})$ can be formulated by a MRF to model contextual dependencies among activation labels. It is assumed that the conditional distribution of an activation label at site x is totally determined by the labels from its neighborhood N_x , i.e., $p(l_x|l_y, y \neq x) = p(l_x|l_y, y \in N_x)$. The prior probability $p(\mathbf{l})$ is given by a Gibbs distribution defined on one-pixel and two-pixel potentials as well

$$p(\mathbf{l}) \propto \exp \left\{ - \sum_{x \in X} \left[V_x(l_x) + \sum_{y \in N_x} V_{x,y}(l_x, l_y) \right] \right\}. \quad (3)$$

For computational tractability, the likelihood (or observation) model $p(\mathbf{d}|\mathbf{l})$ is usually factorized as the product of local likelihoods at individual sites

$$p(\mathbf{d}|\mathbf{l}) = \prod_{x \in X} p(d_x|l_x). \quad (4)$$

Combining the prior model $p(\mathbf{l})$ and the likelihood model $p(\mathbf{d}|\mathbf{l})$, it can be seen that the generative framework considers only the data-independent smoothness constraint. The data-dependent interaction between neighboring sites (the second term in the pairwise potential (2b)) is ignored in the generative framework due to the assumption of conditional independence of observed data in (4). However, the connectivity of neural systems makes the observation from a brain voxel highly dependent on its neighboring sites of the same class. Comparing to the MRF formulation, the CRF approach relaxes the strong assumption of conditional independence for contextual modeling of functional imaging data. The interaction strength between neighboring sites can be adaptively adjusted in terms of their similarity, which enables the CRF approach further explore the contextual dependencies in functional images.

III. BRAIN ACTIVITY DETECTION

In a fMRI time-series with total T ($T \in \mathbf{N}$) image scans, the time-series response of a point x is represented by $(r_x(1), r_x(2), \dots, r_x(T))$, and the input stimulus to the brain is denoted by a binary time-series $(s(1), s(2), \dots, s(T))$. The expression of observation d_x is given later in this section. For the detection of brain activity, each voxel x in the brain is labeled as either activated or inactive. The activation label equals one if the site is activated, otherwise the label equals zero.

The one-pixel potential function is set as $V_x(l_x|\mathbf{d}) = -\ln p(l_x|d_x)$ so that the posterior distribution $p(\mathbf{l}|\mathbf{d})$ becomes the product of local posterior probability $p(l_x|d_x)$ at each site if the two-pixel potential $V_{x,y}(l_x, l_y|\mathbf{d})$ is ignored. Since $p(l_x|d_x) \propto p(l_x, d_x) = p(l_x)p(d_x|l_x)$, the two terms in the one-pixel potential (2a) become $V_x^l(l_x) = -\ln p(l_x)$ and $V_x^{ld}(l_x|\mathbf{d}) = -\ln p(d_x|l_x)$. The prior information of individual classes can be expressed by the following data-independent one-pixel potential

$$V_x^l(l_x = i) = -\ln p(l_x = i) = \alpha_i. \quad (5)$$

The smaller α_i is, the more likely a site x will be labeled as the i th class.

In the detection of brain activity, the temporal response from regions of interest should be impacted by the stimulus signal. Consider the correlation coefficient between the stimulus and the response at a site x

$$c_x = \frac{\sum_t [s(t) - \bar{s}] [r_x(t) - \bar{r}_x]}{\sqrt{\sum_t [s(t) - \bar{s}]^2 \sum_t [r_x(t) - \bar{r}_x]^2}} \quad (6)$$

where $\bar{s} = (1/T) \sum_t s(t)$, $\bar{r}_x = (1/T) \sum_t r_x(t)$, c_x is the correlation coefficient, and $-1 \leq c_x \leq 1$. The value of correlation coefficient will be positive if the brain voxel is activated by the input stimulus. Otherwise its value will be close to zero for an inactive brain voxel. Considering the hemodynamic response of neuron activities, the input stimulus is replaced by the convolution of the stimulus signal and synthetic HRF (the HRF used in the statistical parametric mapping software from <http://www.fil.ion.ucl.ac.uk/spm/>) when calculating correlation coefficients. The multiple correlation analysis or canonical correlation analysis is employed to compute the correlation coefficient when dealing with varying HRFs and multiple stimulus conditions [10]. We represent the observation by using the Fisher's Z transformation

$$d_x = \frac{1}{2} \ln \frac{1 + c_x}{1 - c_x}. \quad (7)$$

The posterior probability of the observation $p(d_x|l_x)$ can be approximated by a zero-mean Gaussian distribution when the site is inactive [1]. Hence

$$\begin{aligned} V_x^{ld}(l_x = 0|\mathbf{d}) &= -\ln p(d_x|l_x = 0) \\ &\approx -\ln N\left(d_x; 0, \frac{1}{T-3}\right) \end{aligned} \quad (8)$$

where $N(z; \mu, \sigma^2)$ represents a Gaussian distribution with variable z , mean μ , and variance σ^2 . When the site is activated by the input stimulus, a uniform distribution is simply assumed as the true distribution of activated voxels is not known

$$V_x^{ld}(l_x = 1|\mathbf{d}) = -\ln p(d_x|l_x = 1) \approx -\ln \frac{1}{c} \quad (9)$$

where $d_x \in (0, c]$, $c = (1/2) \ln[(1 + c_{\max})/(1 - c_{\max})]$, and $c_{\max} = \max_{x \in X} c_x$.

Since activated regions usually consist of contiguous brain voxels, neighboring sites tend to have the same label. The connectivity constraint is imposed by the following data-independent pairwise potential to encourage contiguous detection result

$$V_{x,y}^l(l_x, l_y) \propto 1 - \delta(l_x - l_y) \quad (10)$$

where

$$\delta(z) = \begin{cases} 1, & \text{if } z = 0 \\ 0, & \text{otherwise} \end{cases}$$

is the Kronecker delta function. The pairwise smoothness constraint is imposed only when the two activation labels are different. Thus, neighboring points are more likely to belong to the same class than to different classes.

The data-dependent pairwise potential can be expressed as $V_{x,y}^{ld}(l_x, l_y|\mathbf{d}) = V_{x,y}^l(l_x, l_y|d_x, d_y) \propto |d_x - d_y| \delta(l_x - l_y)$, so that the pairwise constraint encourages data similarity between two neighboring sites when they have the same activation label. However, under heavy noises, neighboring sites may become quite different even though they belong to the same class. To prevent this problem when dealing with the noisy fMRI data, the

data-dependent pairwise potential is replaced by the following normalized term

$$\begin{aligned} V_{x,y}^{ll^d}(l_x, l_y | \mathbf{d}) &= V_{x,y}^{ll^d}(l_x, l_y | d_{N_x}, d_{N_y}) \\ &\propto \frac{|d_x - d_y| \delta(l_x - l_y)}{\frac{1}{|N_x|} \sum_{z \in N_x} |d_x - d_z| + \frac{1}{|N_y|} \sum_{z \in N_y} |d_y - d_z|} \end{aligned} \quad (11)$$

where for a set of points N , $|N|$ denotes the size (number of points) of the set, d_N denotes $\{d_x | x \in N\}$. The pairwise potential models the neighborhood interaction dependent on the observed data. Naturally, the potential imposes an adaptive contextual constraint that adjusts the interaction strength according to the similarity between neighboring observations.

Given the one-pixel and two-pixel potential functions, the maximum *a posteriori* estimation of the activation pattern is given by $\hat{\mathbf{l}} = \arg \max_i p(\mathbf{l} | \mathbf{d})$.

IV. PARAMETERS AND OPTIMIZATION

The potential functions of the posterior probability $p(\mathbf{l} | \mathbf{d})$ are expressed as the following:

$$V_x(l_x | \mathbf{d}) = \begin{cases} -\ln N(d_x; 0, \frac{1}{T-3}), & \text{if } l_x = 0 \\ \alpha + \ln c, & \text{if } l_x = 1 \end{cases} \quad (12a)$$

$$\begin{aligned} V_{x,y}(l_x, l_y | \mathbf{d}) &= \beta_1 (1 - \delta(l_x - l_y)) \\ &+ \frac{\beta_2 |d_x - d_y| \delta(l_x - l_y)}{\frac{1}{|N_x|} \sum_{z \in N_x} |d_x - d_z| + \frac{1}{|N_y|} \sum_{z \in N_y} |d_y - d_z|} \end{aligned} \quad (12b)$$

where $\alpha = \alpha_1 - \alpha_0$. α controls the sensitivity of activity detection, β_1 and β_2 , respectively, weigh the importance of data-independent smoothness constraint and data-dependent neighborhood interaction. To balance the potential terms for the contextual constraints, we assume that

$$\frac{1}{|X|} \sum_{x \in X} \sum_{y \in N_x} \beta_1 = \frac{1}{|X|} \sum_{x \in X} \sum_{y \in N_x} \beta_2 = \gamma^2. \quad (13)$$

The parameter α reflects the influence of prior information for brain activation. The smaller the value of α , the more likely activated regions will be detected. It is empirically set as $1 \leq \alpha \leq 2$ in our experiments. Meanwhile, the parameter γ reflects the influence of contextual constraint from neighboring sites. The higher the value of γ , the stronger contextual constraints are utilized. In our experiments, it is found by trial that $1 \leq \gamma \leq 2$ produces the visually optimal activation pattern for the analysis of fMRI data.

Given the potential functions, the optimization for the posterior probability of the activation pattern is generally difficult due to the data-dependent interactions among neighboring sites. Here, the mean field approximation scheme is employed to get the suboptimal estimate of the activation pattern [19]. The mean field algorithm suggests that when estimating the label mean at

a single site, the influence from neighboring sites can be approximated by that of their means. The activation pattern can be estimated as

$$p(\mathbf{l} | \mathbf{d}) \approx \prod_{x \in X} q_x(l_x | \mathbf{d}) \quad (14a)$$

$$\hat{l}_x = \arg \max_i q_x(l_x = i | \mathbf{d}) \quad (14b)$$

where the mean field local probabilities $\{q_x(l_x | \mathbf{d}) | x \in X\}$ are computed from an iterative procedure (see the Appendix).

V. RESULTS AND DISCUSSION

The present approach was tested on both synthetic and real functional time-series and compared with earlier detection methods. Three brain activity detection algorithms were studied in our experiments: the statistical parametric mapping (SPM) algorithm [12], the MRF algorithm (the proposed algorithm ignoring the data-dependent pairwise potential), and the proposed CRF algorithm. The detected activation by SPM is given by significance values using t-test, whereas those by MRF and CRF are given by the probabilities of activation. The 24-pixel neighborhood for 2-D images and 124-voxel neighborhood for 3-D images were utilized in the experiments (when applicable). All the fMRI data were corrected for motion artifacts as described in [11]. Spatial smoothing was performed with a Gaussian filter of 6 mm FWHM in the SPM approach.

A. Synthetic Data

A 2-D dataset with 64×64 pixels per image scan was generated by using the synthetic functional time-series. The synthetic data totally had 96 images, where the input stimulus consisted of six cycles, each having eight rest samples followed by eight task samples, and the duration between two scans was two seconds ($TR = 2$ s). A box-car time-series was designed for activated pixels, while inactive pixels remained unchanged over time. Then, the response of the activated pixels was generated by convolving the box-car time-series with a gamma HRF ($\text{lag} = 5$ s and $\text{dispersion} = 5$ s). Gaussian random noises were then added to the time-series of both activated and inactive pixels. Pixel intensities of image scans are shown in Fig. 2. The SNR is defined as $\text{SNR} = (h^2/\sigma^2)$, where h is the amplitude of the box-car time-series, and σ is the standard deviation of the noise. Synthetic image series with independent identically distributed (i.i.d.) noises and spatially correlated noises (the average of neighboring i.i.d. Gaussian noises) have been both tested in the synthetic experiments.

Figs. 3–6 show the detection results by SPM, MRF, and CRF approaches for the synthetic functional data under two different noise levels. It can be seen that the three methods show similar performances when the SNR is high. Although most activated points are detected by the SPM approach, details (or high frequency information) of activated regions are blurred by statistical parametric mapping especially under correlated noises when the SNR is low. The MRF approach generates relatively contiguous results by simultaneously performing activity detection and spatial regularization, but the boundaries are still inaccurate due to the neglect of data interaction among neighboring sites. By incorporating interactions of both activation labels and

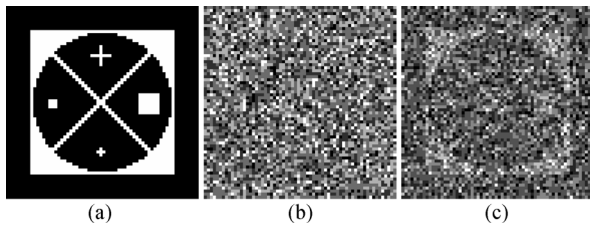


Fig. 2. The synthetic functional images under i.i.d. Gaussian noises with $\text{SNR} = 1.2$: (a) activated regions (in bright), (b) the 40th image scan, and (c) the 80th image scan.

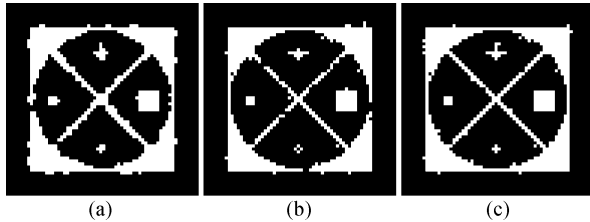


Fig. 3. Detected activation from synthetic functional data by (a) SPM, (b) MRF, and (c) CRF methods under independent noises with $\text{SNR} = 2.0$.

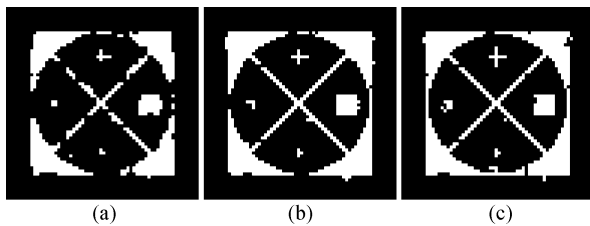


Fig. 4. Detected activation from synthetic functional data by (a) SPM, (b) MRF, and (c) CRF methods under correlated noises with $\text{SNR} = 2.0$.

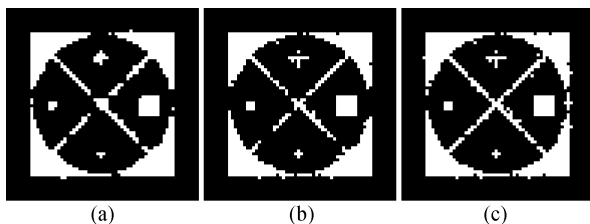


Fig. 5. Detected activation from synthetic functional data by (a) SPM, (b) MRF, and (c) CRF methods under independent noises with $\text{SNR} = 1.2$.

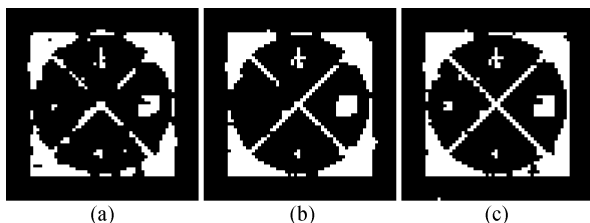


Fig. 6. Detected activation from synthetic functional data by (a) SPM, (b) MRF, and (c) CRF methods under correlated noises with $\text{SNR} = 1.2$.

observed data, the accuracy of activity detection is significantly improved by the proposed CRF approach under noisy environments.

The detection results were also evaluated quantitatively by comparing to the ground-truth image shown in Fig. 2(a). The

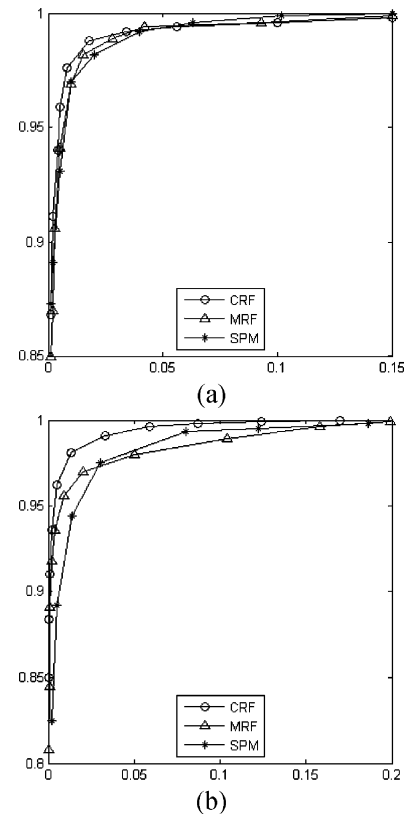


Fig. 7. ROC curves of SPM, MRF, and CRF methods under (a) independent noises and (b) correlated noises with $\text{SNR} = 2.0$.

corresponding receiver operating characteristic (ROC) curves for the three algorithms under two different noise levels are shown in Figs. 7 and 8, where the vertical axis and horizontal axis represent the true positive rate (the portion of activated points that are detected) and the false negative rate (the portion of inactive points that are misclassified) respectively. Compared to the SPM approach and the MRF approach, the CRF approach takes advantage of data-dependent neighborhood interactions, which helps avoid the suppression of high frequency information in functional images and relaxes the strong assumption of conditional independence among observations. The substantial increase of the detection accuracy under correlated noises indicates that the CRF approach effectively fuses contextual constraints in functional images.

Comparing with the SPM algorithm and the MRF algorithm, the CRF algorithm is computationally more complex since it considers contextual constraints among both labels and observations besides the data information at individual sites. Hence the proposed method enhances the performance of activation detection in functional imaging data with a tradeoff in relatively high computational load. The MRF algorithm and the CRF algorithm are both implemented by Visual C. In the experiment, the processing of the synthetic image series respectively took about 2.5 seconds for the MRF algorithm and 4 seconds for the CRF algorithm on a Pentium 4 1.7-GHz PC. The SPM algorithm is implemented by Matlab, and it took about 9 seconds to process the same data.

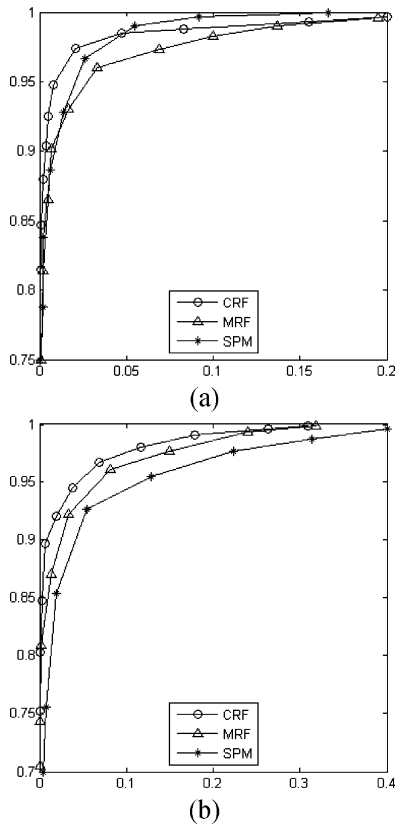


Fig. 8. ROC curves of SPM, MRF, and CRF methods under (a) independent noises and (b) correlated noises with SNR = 1.2.

B. Visual Stimulation Task

The detection algorithms were tested on real fMRI data gathered on visual stimulation task where for each subject, 64 brain scans with three 2-D T2-weighted slices (128 × 64 points in each slice, zero filled to 128 × 128 points) per image scan were acquired by using a gradient-echo FLASH sequence (TR = 5 s, TE = 40 ms). In the experiment, ON and OFF stimuli were presented at a rate of 5.16 s per sample. Each stimulation period had four successive stimulation ON samples followed by four stimulation OFF samples. The stimulations were repeated for eight cycles, and experiments were carried out at different sessions with different subjects. An 8-Hz alternating checkerboard pattern with a central fixation point was projected on a LCD system, and the subject was asked to fixate on the point during stimulations. Further details of the visual simulation experiments can be found in [23].

Fig. 9 shows the detected activation from fMRI data gathered on the visual stimulation task performed by a representative subject. The results of other subjects were similar. Although activated visual cortex areas were detected by all the three approaches, the detection by the CRF method is relatively elaborate due to the relaxation of the strong assumption of conditional independence among observed data. Fig. 10 shows the normalized neighborhood interactions (the exponential of the data-dependent pairwise potential) for some activated and inactive brain voxels within their neighborhoods. It can be seen that the interaction strength is adaptively adjusted according to the similarity

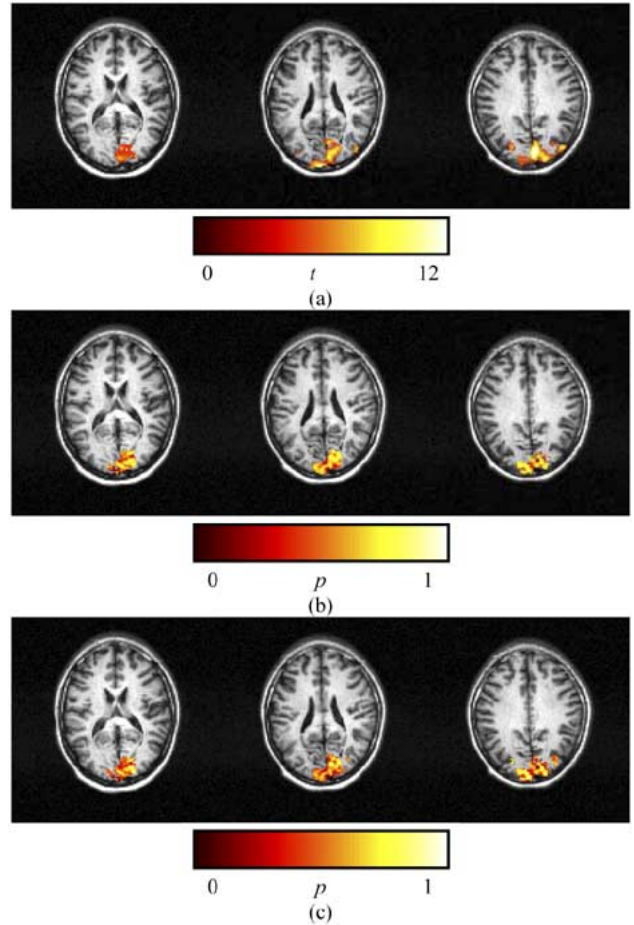


Fig. 9. Detected activation on three axial brain slices by (a) SPM, (b) MRF, and (c) CRF methods from fMRI data of a representative subject performing the visual stimulation task.

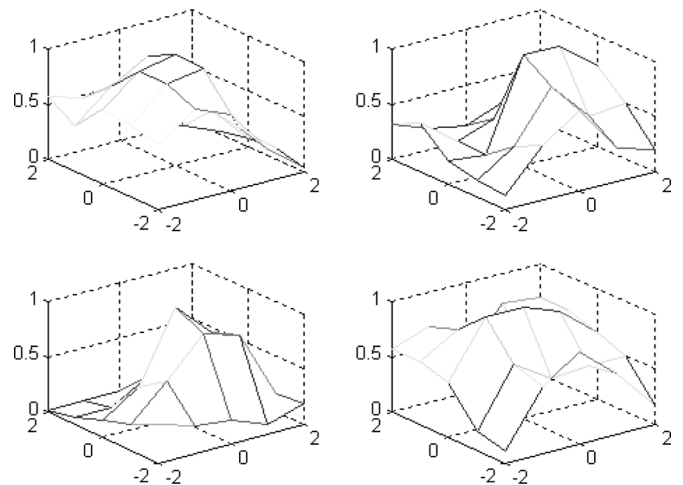


Fig. 10. Data-dependent interactions of brain voxels within their neighborhoods.

between the central point and its neighboring sites, resulting in various interaction patterns within the detection process.

C. Memorial Retrieval Task

In this experiment, for each subject a fMRI time-series of 864 brain scans with eight slices (64 × 64 × 8 voxels per scan) was

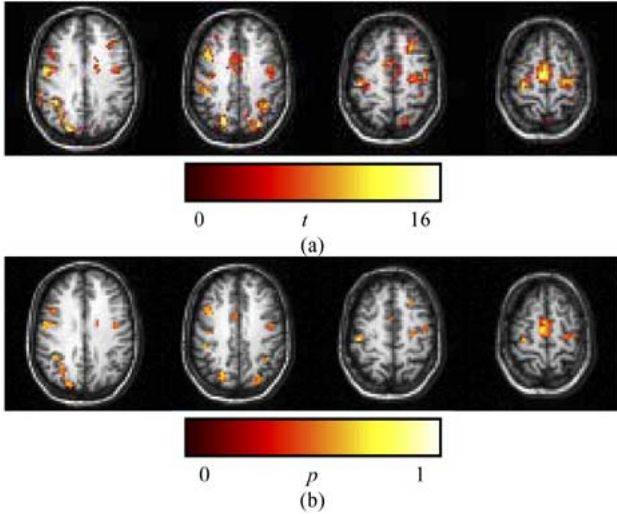


Fig. 11. Detected activation on four axial brain slices by (a) SPM and (b) CRF methods from fMRI data of a representative subject performing the memory retrieval task.

acquired using a gradient-echo EPI sequence ($TR = 1$ s, $TE = 40$ ms). In the experiment, subspan sets of 3–6 alphabet letters excluding the letter Y were presented visually for two seconds, then a probe letter appeared after a variable delay length. Subjects were required to decide if the probe letter belonged to a previously presented subspan set. All trial combinations were presented randomly in a single run, at an inter-trial interval of 18 s. Further details of the experiments can be found in [16].

Fig. 11 shows the detected activation from fMRI data gathered on the memory retrieval task by the proposed approach and the statistical parametric mapping approach. Expected brain areas such as middle frontal gyrus (BA 9/46), inferior frontal gyrus (BA 44/45), superior parietal cortex (BA 5/7), supplementary motor area (BA 6), and primary motor cortex (BA 4) were detected by both methods. As seen, compared to the results by SPM, the activated areas detected by the CRF approach are relatively contiguous and concentrative. Furthermore, the activation patterns detected by the proposed method contain less spurious noises.

D. Silent Reading Task

In this experiment, for each subject, 360 brain scans with 35 slices ($64 \times 64 \times 35$ voxels per scan) were acquired using an EPI sequence ($TR = 3.15$ s, $TE = 40$ ms). The experimental task involved alternative reading of words and pseudo-words with variable presenting frequencies, and the resting condition involved fixating a cross in the middle of the screen. Each trial lasted 21 s and was followed by a resting period of 16 s. More details of the experiments can be found in [21].

Fig. 12 shows the results of activity detection from fMRI data gathered on the silent reading task by the CRF approach and the SPM approach. It can be seen that the detection results by the proposed algorithm are consistent with those by the statistical parametric mapping method. Expected activation in related brain regions including extrastriate cortex (BA 18/19), superior parietal lobule (BA 7), middle temporal cortex (BA 21/22), inferior frontal gyrus (BA 44/45), and middle frontal gyrus (BA 9/46) were found by both methods.

Due to the lack of ground truth, it is hard to quantitatively determine which method is more accurate by mere visualization of the detection results with real functional imaging data. Overall, the CRF approach outperforms the other two methods in the synthetic experiments and robustly detects brain activities in the real fMRI data with less spurious noises and more elaborate boundaries by integrating contextual constraints within both activation labels and observed data.

VI. CONCLUSION

We presented a probabilistic discriminative approach to fuse contextual constraints in functional images based on the CRF and applied it to the detection of brain activation from both synthetic and real fMRI data. The neural activities are modulated by hemodynamic responses and corrupted by scanner noises. Thus far, the temporal correlation of activation responses has been considered. The spatial dependencies of the data are caused by the coupling of hemodynamic responses and correlation of scanner noises. The CRF provides an effective approach to model the contextual dependencies of both labels and data. Compared to earlier work including SPM and MRF approaches, the CRF approach takes the advantage of data-dependent interactions within functional imaging data and significantly improves the performance of the detection of brain activity. In our experiments with synthetic data, the ROC curves showed that detection accuracy was substantially increased especially under correlated noises. With the real fMRI data, the detection results by the proposed method were visually either similar or better in the sense of details and localization to cortical areas, compared to the other methods. The improvement indicates that it is important to consider contextual dependencies of the observations in addition to those among the labels or neural activities when studying fMRI data. To further enhance the efficiency of the proposed technique, our future work focuses on automatically determining all the parameters and applying the algorithm to the study of connectivity among activated regions.

APPENDIX

The mean field local energy for site x is defined as

$$U_x(l_x|\mathbf{d}) = V_x(l_x|\mathbf{d}) + \sum_{y \in N_x} V_{x,y}(l_x, \langle l_y \rangle | \mathbf{d}) \quad (15)$$

where $\langle \cdot \rangle$ denotes the expectation or ensemble average. The conditional probability for site x is approximated by the mean field local probability

$$q_x(l_x|\mathbf{d}) = Q_x^{-1} \exp[-U_x(l_x|\mathbf{d})] \quad (16)$$

where Q_x is called the mean field local partition

$$Q_x = \sum_{l_x} \exp[-U_x(l_x|\mathbf{d})]. \quad (17)$$

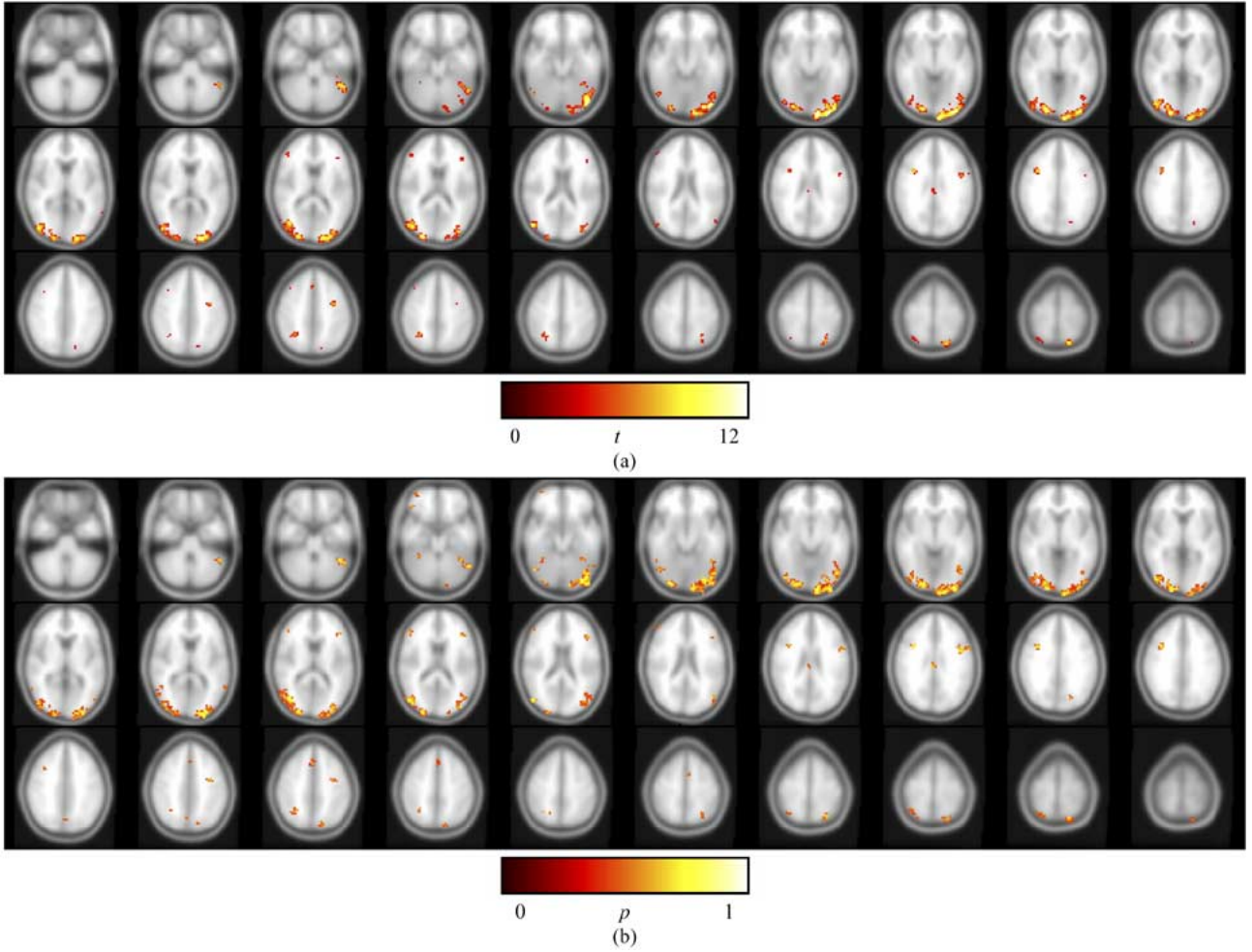


Fig. 12. Detected brain activation by (a) SPM and (b) CRF methods from fMRI data of a representative subject performing the silent reading task.

Hence, the mean of an activation label is computed as

$$\begin{aligned} \langle l_x \rangle &\approx \sum_{l_x} l_x q_x(l_x | \mathbf{d}) \\ &= Q_x^{-1} \sum_{l_x} l_x \exp[-U_x(l_x | \mathbf{d})]. \end{aligned} \quad (18)$$

It can be seen that in order to find the mean of a site, one has to know the means of its neighbors. Therefore, the mean of the activation pattern can be iteratively estimated using (15), (17), and (18). Initially, $q_x(l_x = i)$ is set as $1/L$ for all i and x . Given the label means, the posterior distribution of the activation pattern is approximated by the product of mean field local probabilities

$$p(\mathbf{l} | \mathbf{d}) \approx \prod_{x \in X} q_x(l_x | \mathbf{d}) = \prod_{x \in X} Q_x^{-1} \exp[-U_x(l_x | \mathbf{d})]. \quad (19)$$

ACKNOWLEDGMENT

The authors thank Dr. F. Kruggel for providing the visual stimulation and memory retrieval experiment data at the Max-Planck-Institute of Cognitive Neuroscience, Leipzig, Germany. The silent reading data set is supported by the fMRI Data Center (fMRIDC), Dartmouth College, Dartmouth, MA (available at <http://www.fmridc.org>).

REFERENCES

- [1] B. A. Ardekani and I. Kanno, "Statistical methods for detecting activated regions in functional MRI of the brain," *Magn. Reson. Imag.*, vol. 16, pp. 1217–1225, 1998.
- [2] P. A. Bandettini, A. Jesmanowicz, E. C. Wong, and J. S. Hyde, "Processing strategies for time-course data sets in functional MRI of the human brain," *Magn. Reson. Med.*, vol. 30, pp. 161–173, 1993.
- [3] J. Besag, "Spatial interaction and the statistical analysis of lattice systems," *J. Roy. Statist. Soc. B*, vol. 36, pp. 192–236, 1974.
- [4] —, "On the statistical analysis of dirty pictures," *J. Roy. Statist. Soc. B*, vol. 48, pp. 259–302, 1986.
- [5] V. D. Calhoun, T. Adali, G. D. Pearlson, and J. J. Pekar, "Spatial and temporal independent component analysis of functional MRI data containing a pair of task-related waveforms," *Hum. Brain Mapp.*, vol. 13, pp. 43–53, 2001.
- [6] E. R. Cosman, J. W. Fisher, and W. M. Wells, "Exact MAP activity detection in fMRI using a GLM with an ising spatial prior," in *Proc. Int. Conf. Medical Image Computing and Computer-Assisted Intervention*, 2004, vol. 2, pp. 703–710.
- [7] X. Descombes, F. Kruggel, and D. Y. von Cramon, "Spatio-temporal fMRI analysis using Markov random fields," *IEEE Trans. Med. Imag.*, vol. 17, no. 6, pp. 1028–1039, Dec. 1998.
- [8] B. S. Everitt and E. T. Bullmore, "Mixture model mapping of brain activation in functional magnetic resonance images," *Hum. Brain Mapp.*, vol. 7, pp. 1–14, 1999.
- [9] S. Faisan, L. Thoraval, J.-P. Arnschach, M.-N. Metz-Lutz, and F. Heitz, "Unsupervised learning and mapping of active brain functional MRI signals based on hidden semi-Markov event sequence models," *IEEE Trans. Med. Imag.*, vol. 24, no. 2, pp. 263–276, Feb. 2005.

- [10] O. Friman, J. Cedefamn, P. Lundberg, M. Borga, and H. Knutsson, "Detection of neural activity in functional MRI using canonical correlation analysis," *Magn. Reson. Med.*, vol. 45, pp. 323–330, 2001.
- [11] K. J. Friston, J. Ashburner, C. D. Frith, J.-B. Poline, J. D. Heather, and R. S. J. Frackowiak, "Spatial registration and normalization of images," *Hum. Brain Mapp.*, vol. 3, pp. 165–189, 1995.
- [12] K. J. Friston, A. P. Holmes, J.-B. Poline, P. J. Grasby, S. C. R. Williams, R. S. J. Frackowiak, and R. Turner, "Analysis of fMRI time-series revisited," *NeuroImage*, vol. 2, pp. 45–53, 1995.
- [13] C. Goutte, P. Toft, E. Rostrup, F. A. Nielsen, and L. K. Hansen, "On clustering fMRI time series," *Neuroimage*, vol. 9, pp. 298–310, 1999.
- [14] L. K. Hansen, J. Larsen, F. A. Nielsen, S. C. Strother, E. Rostrup, R. Savoy, N. Lange, J. Sidtis, C. Svarer, and O. B. Paulson, "Generalizable patterns in neuroimaging: how many principal components?," *NeuroImage*, vol. 9, pp. 534–544, 1999.
- [15] N. V. Hartvig and J. L. Jensen, "Spatial mixture modeling of fMRI data," *Hum. Brain Mapp.*, vol. 11, pp. 233–248, 2000.
- [16] F. Kruggel, S. Zysset, and D. Y. von Cramon, "Nonlinear regression of functional MRI data: an item recognition task study," *Neuroimage*, vol. 12, pp. 173–183, 2000.
- [17] S. Kumar and M. Hebert, "Discriminative fields for modeling spatial dependencies in natural images," *Adv. Neural Inf. Process. Syst.*, pp. 1351–1358, 2004.
- [18] J. Lafferty, A. McCallum, and F. Pereira, "Conditional random fields: probabilistic models for segmenting and labeling sequence data," in *Proc. Int. Conf. Machine Learning*, 2001, pp. 282–289.
- [19] S. Z. Li, *Markov Random Field Modeling in Image Analysis*. Berlin, Germany: Springer-Verlag, 2001.
- [20] G. Marrelec, P. Ciuciu, M. Pelegrini-Issac, and H. Benali, "Estimation of the hemodynamic response function in event-related functional MRI: directed acyclic graphs for a general Bayesian framework," in *Proc. Information Processing in Medical Imaging Conf.*, 2003, pp. 635–646.
- [21] A. Mechelli, K. J. Friston, and C. J. Price, "The effects of presentation rate during word and pseudoword reading: a comparison of PET and fMRI," *Cogn. Neurosc.*, vol. 12, pp. 145–156, 2000.
- [22] T. E. Nichols and A. P. Holmes, "Nonparametric permutation tests for functional neuroimaging: a primer with examples," *Hum. Brain Mapp.*, vol. 15, pp. 1–25, 2001.
- [23] J. C. Rajapakse, F. Kruggel, J. M. Maisog, and D. Y. von Cramon, "Modeling hemodynamic response for analysis of functional MRI time-series," *Hum. Brain Mapp.*, vol. 6, pp. 283–300, 1998.
- [24] J. C. Rajapakse and J. Piyaratna, "Bayesian approach to segmentation of statistical parametric maps," *IEEE Trans. Biomed. Eng.*, vol. 48, no. 10, pp. 1186–1194, Oct. 2001.
- [25] E. Salli, H. J. Aronen, S. Savolainen, A. Korvenoja, and A. Visa, "Contextual clustering for analysis of functional MRI data," *IEEE Trans. Med. Imag.*, vol. 20, no. 5, pp. 403–414, May 2001.
- [26] M. Svendsen, F. Kruggel, and D. Y. von Cramon, "Probabilistic modeling of single-trial fMRI data," *IEEE Trans. Med. Imag.*, vol. 19, no. 1, pp. 25–35, Jan. 2000.
- [27] Y. Wang and Q. Ji, "A dynamic conditional random field model for object segmentation in image sequences," in *Proc. IEEE Conf. Computer Vision and Pattern Recognition*, 2005, vol. 1, pp. 264–270.
- [28] M. W. Woolrich, T. E. J. Behrens, C. F. Beckmann, and S. M. Smith, "Mixture models with adaptive spatial regularization for segmentation with an application to fMRI data," *IEEE Trans. Med. Imag.*, vol. 24, no. 1, pp. 1–11, Jan. 2005.